Available online at www.sciencedirect.com
SCIENCE DIRECT
Physica D 217 (2006) 153–160
PHYSICA D
www.elsevier.com/locate/physd

Multi phase field model for solid state transformation with elastic strain

I. Steinbach*, M. Apel

RWTH-Aachen, Access e.V., Intzestrasse 5, 52070 Aachen, Germany

Received 12 August 2005; received in revised form 14 December 2005; accepted 3 April 2006
Available online 8 May 2006
Communicated by M. Vergassola

Abstract

A multi phase field model is presented for the investigation of the effect of transformation strain on the transformation kinetics, morphology and thermodynamic stability in multi phase materials. The model conserves homogeneity of stress in the diffuse interface between elastically inhomogeneous phases, in which respect it differs from previous models. The model is formulated consistently with the multi phase field model for diffusional and surface driven phase transitions [I. Steinbach, F. Pezzolla, B. Nestler, M. Seeßelberg, R. Prieler, G.J. Schmitz, J.L.L. Rezende, A phase field concept for multiphase systems, Physica D 94 (1996) 135–147; J. Tiaden, B. Nestler, H.J. Diepers, I. Steinbach, The multiphase-field model with an integrated concept for modeling solute diffusion, Physica D 115 (1998) 73–86; I. Steinbach, F. Pezzolla, A generalized field method for multiphase transformations using interface fields, Physica D 134 (1999) 385] and gives a consistent description of interfacial tension, multi phase thermodynamics and elastic stress balance in multiple junctions between an arbitrary number of grains and phases. Some aspects of the model are demonstrated with respect to numerical accuracy and the relation between transformation strain, external stress and thermodynamic equilibrium.

Keywords: Phase field models; Solid state transformation; Elasticity; Simulation

1. Introduction

The microstructure of multi phase materials like steel, Ni-base superalloys or precipitation hardened aluminum is known to be the key parameter to determine the materials properties. The factors controlling the microstructure formation thereby range from atomic ordering to the macroscopic conditions of production processes. To describe the complex interactions between atomistic mechanisms and macroscopic conditions on the mesoscopic scale of the microstructure, the phase field method, or time-dependent Ginzburg–Landau method as it was called in early publications, has turned out to be the method of choice. Certainly, the school of Khachaturyan has formed the field by demonstrating the applicability of the method to various solid state systems (for an actual review on the field, see [4]). In contrast to sharp interface models, the necessity of tracking the interface between different phases during transformation is dispensed by the evaluation of the phase field contour. Furthermore, the balance of stress and strain at the moving boundary is substituted by treating the different phases and the interfaces between them as one domain with effective material properties, varying over the interface. The convergence of the approach to the respective sharp interface limit is discussed in detail in [5].

The phase field method starts very generally from an Onsager kinetic equation for the temporal evolution of a set of continuum field variables $\Psi_\alpha(x^i, t)$ defined in space x^i and time t:

$$\dot{\Psi}_\alpha = -\sum_\beta M^{\Psi}_{\alpha\beta} \frac{\delta F}{\delta \Psi_\beta} \tag{1}$$

where F is an appropriate functional measuring the state of the system. $M^{\Psi}_{\alpha\beta}$ is a relaxation matrix for non-conserved fields or a relaxation operator, proportional to the divergence in space, for conserved fields. The functional variable Ψ_α can be identified with the structural order parameter or "phase field" ϕ_α, with temperature T, concentration $\vec{c}$, total strain ϵ^{ij}, magnetization m^i or other variables relevant to describe the system of interest. Each field again can be a scalar, a vector

* Corresponding author. Tel.: +49 2418098012; fax: +49 24138578.
E-mail address: i.steinbach@access.rwth-aachen.de (I. Steinbach).

0167-2789/$ - see front matter © 2006 Elsevier B.V. All rights reserved.
doi:10.1016/j.physd.2006.04.001

or a tensor (throughout the paper, we will keep the convention of using Greek characters for different phases, small Latin characters for the spatial directions, and the vector symbol for the concentrations). However, already Eq. (1) is under heavy debate if applied to an interface in solid state material, where details of the atomistic structure certainly play a significant role. Therefore a clear distinction of the scales is needed to guarantee the applicability of the method. This distinction was one main reason for the development of the multi phase field method, as will be described in Section 2. After the general frame is set, the multi phase field model with elastic strain is defined in Sections 3 and 4. The approach is similar to the one of Dreyer and Müller [6], who expand the elastic parameters as a function of the phase state rather than a function of the concentration, as in Khachaturyans model [4]. Numerical tests are shown in Sections 5 and 6. They deal with application of the model to investigate the effect of transformation strain on the γ/α transformation in steel.

2. Thin interfaces in multi phase systems

Here we adopt the terminology that a "thin" interface is thin compared to the typical scale of the microstructure $\overline{r}$, but its width η is large compared to the atomic distance a:

$$a \ll \eta \ll \overline{r}. \tag{2}$$

Obviously, a numerical calculation with an interface width η, large compared to the physical width of order a, will lose its quantitative correctness if the results depend on η. In order to perform quantitative calculations, one then has to:

(a) resolve the physical dimension of the interface;

(b) modify the model in order to become independent of η, but capture the physics of interest—then the interface width can be scaled for numerical convenience.

Here, we will follow route (b), which starts from the work of Caginalp et al. about motion driven by mean curvature and the sharp interface limit of thin interface models [7,8]. One further step on this route is the thin interface kinetic correction by Karma and coworkers [9,10]. In order to capture realistic phase diagrams avoiding spurious interface energies, the multi phase field model was developed by the group of the authors [2] and further developed by Kim et al. [11]. The basis of the model is a formal coarse graining procedure from the atomistic interface to a mesoscopic interface having a thin width η, illustrated in the following way. Compared to the scale of numerical resolution, the physical interface appears to be a sharp interface, which is characterized by a discontinuity of the materials properties between the phases on both sides of the interface. The continuum field variables Ψ are therefore split into the variables Ψ_α and Ψ_β related to the phases α and β inside the interface. As the actual position of the (physical) interface within the thin interface region is uncertain, with an uncertainty η, both variables Ψ_α and Ψ_β are treated as overlapping in the interface (see Fig. 1).

In particular, the concentration field is represented by the phase concentrations $\vec{c}_\alpha$ which are defined in the individual phase regions and overlapping in the interface. To connect the

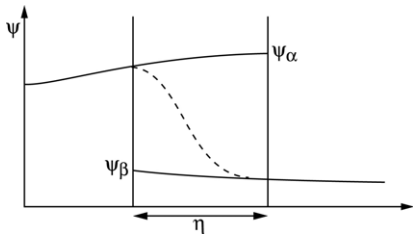

Fig. 1. Schematic representation of the field variable Ψ split into the contributions Ψ_α and Ψ_β related to the phases α and β inside the interface. The dashed line represents the mixture of the phase variable.

discontinuous phase concentrations, we will later apply the assumption of equal chemical potential in the interface. We define the mixture concentration $\vec{c}$, which is continuous over the interface by introducing the phase field variables ϕ_α:

$$\vec{c} = \sum_\alpha \phi_\alpha \vec{c}_\alpha. \tag{3}$$

$\phi_\alpha = 1$ in the bulk phase α, $\phi_\alpha = 0$ in the other bulk phases, and showing a smooth transition in the interfaces connected to phase α. The mixture concentration $\vec{c}$ will be used to evaluate the diffusion fluxes in the numerical calculation (see below). The same approach will now be adopted for the problem with total strain ϵ^{ij} in the directions i, j in three-dimensional space as a function of the phase strain ϵ_α^{ij} in the individual phases:

$$\epsilon^{ij} = \sum_\alpha \phi_\alpha h_\alpha(\epsilon_\alpha^{ij}). \tag{4}$$

The function h_α will depend on the elastic properties of the different phases and, in general, will not be unity. We will employ the assumption of mechanical equilibrium, which is the mechanical analogue to the assumption of equal chemical potentials between the phases, to define this function in general for interfaces and multiple junctions. This will be treated in the next section.

3. The mechanical multi phase model

We start from a general model of the free energy as an integral of the density functional over the domain Ω. The density functional is split into three parts: the grain boundary energy density f^{GB}; the chemical free energy density f^{CH}; and the elastic energy density f^{EL}:

$$F = \int_\Omega f^{\mathrm{GB}} + f^{\mathrm{CH}} + f^{\mathrm{EL}} \tag{5}$$

$$f^{\mathrm{GB}} = \sum_{\alpha,\beta=1}^{N} \frac{4\sigma_{\alpha\beta}}{\eta_{\alpha\beta}} \left\{ \frac{\eta_{\alpha\beta}^2}{\pi^2} \mid \nabla\phi_\alpha \cdot \nabla\phi_\beta \mid + W_{\alpha\beta} \right\}. \tag{6}$$

$\sigma_{\alpha\beta}$ is the grain boundary energy between phase α and phase β in a multi phase junction with N phases, or between grains of the same phase but different orientations. $\eta_{\alpha\beta}$ is the interface width and $W_{\alpha\beta} = \phi_\alpha\phi_\beta$ for $0 < \phi_{\alpha/\beta} < 1$ and ∞ elsewhere is the repulsive (dimensionless) potential function that keeps the interface upright (see [3]). The special form of Eq. (6) was chosen to underline the scaling invariance of the total interface

energy as an integral over f^{GB} with respect to the interface width $\eta_{\alpha\beta}$ (in the thin interface limit): the expression in the brackets is a dimensionless measure of the structure of the interface, while the division of the interfacial energy by the interface width defines the prefactor as a volumetric energy density.

The chemical part of the free energy density is:

$$f^{\mathrm{CH}} = \sum_{\alpha=1}^{N} \phi_\alpha f_\alpha(\vec{c}_\alpha) + \vec{\mu}\left(\vec{c} - \sum_{\alpha=1}^{N} \phi_\alpha \vec{c}_\alpha\right) \tag{7}$$

where $f_\alpha(\vec{c}_\alpha)$ are the bulk free energies of the individual phases, dependent on the phase concentrations $\vec{c}_\alpha$; and $\vec{\mu}$ is the generalized chemical potential vector that is introduced as a Lagrange multiplier to conserve the mass balance between the phases (Eq. (3)).

In the same way, the elastic part of the free energy will be defined on the basis of the elastic properties and variables related to the different phases: the total strain ϵ_α^{ij} in phase α, the eigenstrain ϵ^{*ij}_α, and the elasticity or Hook's matrix C_α^{ijkl}:

$$f^{\mathrm{EL}} = \frac{1}{2}\left\{\sum_{\alpha=1}^{N} \phi_\alpha(\epsilon_\alpha^{ij} - \epsilon^{*ij}_\alpha) C_\alpha^{ijkl}(\epsilon_\alpha^{kl} - \epsilon^{*kl}_\alpha)\right\}. \tag{8}$$

In general, ϵ^{*ij}_α and C_α^{ijkl} are concentration- and temperature-dependent quantities. However, in this paper we restrict ourselves to the case where these quantities are constant in concentration and temperature, but differ for the individual phases. The ansatz (8) is a direct extension of the original multi phase model for diffusive phase transformations, as the total elastic energy is a linear summation of the elastic energies of the individual phases, weighted by the phase densities ϕ_α. To close the problem, an additional condition is needed to correlate the strain fields in the different phases. We may note here that the elastic stresses $\sigma_\alpha^{ij} = \frac{1}{\phi_\alpha}\frac{\partial f^{\mathrm{EL}}}{\partial \epsilon_\alpha^{ij}}$ are the analogue of the generalized chemical potentials in the solutal case $\vec{\mu} = \frac{\partial f^{\mathrm{CH}}}{\partial \vec{c}}$. Equal elastic stresses in the interface are postulated, i.e. mechanical equilibrium between the phases in the strong form with a continuity of all stress components σ^{ij}:

$$\sigma_\alpha^{ij} = \sigma_\beta^{ij} = \sigma^{ij} \tag{9}$$

for all α, β. Equivalently, we have

$$(\epsilon_\alpha^{ij} - \epsilon^{*ij}_\alpha) C_\alpha^{ijkl} = (\epsilon_\beta^{ij} - \epsilon^{*ij}_\beta) C_\beta^{ijkl} =: (\epsilon^{ij} - \epsilon^{*ij}) C^{ijkl} \tag{10}$$

$$\epsilon^{ij} - \epsilon^{*ij} = \sigma^{kl}[C^{ijkl}]^{-1} \tag{11}$$

where we have introduced the effective eigenstrain ϵ^{*ij} and the effective elasticity matrix C^{ijkl}. A linear mixture model for the effective strain $\epsilon^{ij} - \epsilon^{*ij}$ and the effective compliance matrix $[C^{ijkl}]^{-1}$

$$\epsilon^{ij} - \epsilon^{*ij} = \sum_{\alpha=1}^{N} \phi_\alpha(\epsilon_\alpha^{ij} - \epsilon^{*ij}_\alpha) \tag{12}$$

$$[C^{ijkl}]^{-1} = \sum_{\alpha=1}^{N} \phi_\alpha [C_\alpha^{ijkl}]^{-1} \tag{13}$$

defines the effective elasticity matrix

$$C^{ijkl} = \left[\sum_{\alpha=1}^{N} \phi_\alpha [C_\alpha^{ijkl}]^{-1}\right]^{-1}. \tag{14}$$

The elastic energy (8) now reduces to the simple form

$$f^{\mathrm{EL}} = \frac{1}{2}(\epsilon^{ij} - \epsilon^{*ij}) C^{ijkl}(\epsilon^{kl} - \epsilon^{*kl}) \tag{15}$$

where ϵ^{*ij} and C^{ijkl} are effective material properties, continuously varying between the respective properties of the bulk phases. Obviously, the elastic energy Eq. (15) is no longer a linear function in ϕ_α (as in the ansatz Eq. (8)) because the constraint of mechanical equilibrium between the phases is considered explicitly in the model.

It may be noted that the expression (14) is known as the Reuss limit for the elastic behaviour of a compound [12,13]. This limit is adopted as a materials model for the interfaces and junctions. It is known to favour the elastically soft components. The opposite limit (Voigt limit [14,13]) is applied in the model of [6] and [15], where the strain between the phases is continuous and the effective elasticity matrix is an arithmetic mean of the elasticity matrices of the individual phases. The meaning of both models in cases where the elastic properties of the phases differ strongly has to be the subject of further examination. In the sharp interface limit, both models show the correct behaviour of continuous normal stress and discontinous tangential stress (see also Section 5).

4. Kinetic equations and solution procedure

Using the model of the free energy density as a function of the field variables $\phi_\alpha(x,t)$, $\vec{c}(x,t)$ and $\epsilon^{ij}(x,t)$, as defined in the previous section, we postulate the following forms of the kinetic equations:

$$\dot{\phi}_\alpha = -\sum_{\beta=1}^{N} \frac{\mu_{\alpha\beta}}{N}\left(\frac{\delta F}{\delta \phi_\alpha} - \frac{\delta F}{\delta \phi_\beta}\right) \tag{16}$$

$$\dot{\vec{c}} = \nabla\left(\sum_{\alpha=1}^{N} \vec{\vec{M}} \nabla \frac{\delta F}{\delta \vec{c}}\right) \tag{17}$$

$$0^i = \nabla^j \sigma^{ij} = \nabla^j \frac{\delta F}{\delta \epsilon^{ij}} \tag{18}$$

with the interface mobilities $\mu_{\alpha\beta}$ and the chemical mobility matrix $\vec{\vec{M}}$. The division by the vector concentration in Eq. (17) and elsewhere in the text denotes the vector of division by components. The notation of the spatial derivation $\nabla = \nabla^i = \frac{\partial}{\partial x^i}$ is introduced for readability and clarity. The stress strain equation (18) is considered in the static limes of mechanical equilibrium.

Using a double obstacle potential [3], the multi phase field equation (16) yields

$$\dot{\phi}_\alpha = \sum_{\beta=1}^{N} \frac{\mu_{\alpha\beta}}{N}\left\{\sum_{\gamma=1}^{N}[\sigma_{\beta\gamma} I_{\beta\gamma} - \sigma_{\alpha\gamma} I_{\alpha\gamma}] + \Delta G_{\alpha\beta}\right\} \tag{19}$$

$$I_{\alpha\gamma} = \frac{8}{\eta_{\alpha\gamma}}\left[\delta_\alpha \frac{\eta_{\alpha\gamma}^2}{\pi^2}\nabla^2\phi_\gamma + \delta_\alpha\phi_\gamma\right]. \tag{20}$$

The $I_{\alpha\beta}$ are the generalized curvature terms where $\delta_\alpha = 0$ if $\phi_\alpha = 0$ and $\delta_\alpha = 1$ otherwise.[1] $\Delta G_{\alpha\beta}$ is the local deviation from thermodynamic equilibrium, consisting of the chemical part $\Delta G_{\alpha\beta}^{\mathrm{CH}}$ and the elastic part $\Delta G_{\alpha\beta}^{\mathrm{EL}}$, $\Delta G_{\alpha\beta} = \Delta G_{\alpha\beta}^{\mathrm{CH}} + \Delta G_{\alpha\beta}^{\mathrm{EL}}$:

$$\Delta G_{\alpha\beta}^{\mathrm{CH}} = -\left(\frac{\partial}{\partial\phi_\alpha} - \frac{\partial}{\partial\phi_\beta}\right) f^{\mathrm{CH}} \tag{21}$$

$$= -f_\alpha(\vec{c}_\alpha) + f_\beta(\vec{c}_\beta) + \vec{\mu}(\vec{c}_\alpha - \vec{c}_\beta). \tag{22}$$

The phase concentrations $\vec{c}_\alpha$ and the generalized chemical potential $\vec{\mu}$ are calculated iteratively for a given average concentration $\vec{c}$ and a given set of phase fields $\{\phi_\alpha\}$ by minimizing the total free energy using given free energy functions $f_\alpha(\vec{c}_\alpha)$. These are conveniently taken from a thermodynamic data base. Here it shall only be noted that this minimization does not imply that the system is in equilibrium, as the phase densities $\{\phi_\alpha\}$ in general during the transformation do not coincide with equilibrium fractions. Details will be published elsewhere [16].

The elastic non-equilibrium contribution is calculated in the same way:

$$\Delta G_{\alpha\beta}^{\mathrm{EL}} = -\left(\frac{\partial}{\partial\phi_\alpha} - \frac{\partial}{\partial\phi_\beta}\right) f^{\mathrm{EL}} \tag{23}$$

$$= (\epsilon^{ij} - \epsilon^{*ij})C^{ijkl}\left\{(\epsilon^{*kl}_\alpha - \epsilon^{*kl}_\beta) - \frac{1}{2}\left(([C_\alpha^{klmn}]^{-1} - [C_\beta^{klmn}]^{-1})\right)C^{mnop}(\epsilon^{op} - \epsilon^{*op})\right\}. \tag{24}$$

The first part in (24) accounts for the difference in eigenstrain between the phases and the second part for the difference in elasticities. The first part is linearly dependent on the local elastic stress state $(\epsilon^{ij} - \epsilon^{*ij})\bar{C}^{ijkl}$, with the consequence that a phase transition with expansion or contraction can be favored or hindered, depending on the sign of the local stress. The second part, however, is a quadratic form of the stress, with the consequence that (neglecting effects of anisotropy) the elastic weak component is favored if the interface is under load, regardless of the sign of the load. These differences in the functional dependences can be used to separate the two distinct contributions, e.g. in an experimental tensile testing.

Neglecting any stress effect on diffusion, the diffusion equation (17) can be reformulated:

$$\dot{\vec{c}} = \nabla\left(\sum_{\alpha=1}^{N}\phi_\alpha\vec{\vec{M}}_\alpha\nabla\frac{\partial f_\alpha}{\partial\vec{c}_\alpha}\right) = \nabla\left(\sum_{\alpha=1}^{N}\phi_\alpha\vec{\vec{D}}_\alpha\nabla\vec{c}_\alpha\right) \tag{25}$$

with chemical mobility matix $\vec{\vec{M}} = \sum_{\alpha=1}^{N}\phi_\alpha\vec{\vec{M}}_\alpha$ and the diffusion matrices $\vec{\vec{D}}_\alpha = \vec{\vec{M}}_\alpha(\frac{\partial^2 f_\alpha}{\partial\vec{c}_\alpha\partial\vec{c}_\alpha})$. The equivalence of (25) with (17) already implies that the generalized chemical potential $\vec{\mu}$ introduced in (7) is equal in all phases in interfaces and junctions:

$$\vec{\mu} = \frac{\partial f_\alpha}{\partial\vec{c}_\alpha} = \frac{\partial f_\beta}{\partial\vec{c}_\beta} \tag{26}$$

for all α and β. This is assumed to hold close to the local equilibrium of the phases, to which case we shall restrict ourselves. Using the parallel tangent rule (26), the quasi-equilibrium concentrations $\vec{c}^{\,0}_{\alpha\beta}$[2] in a pair of phases α and β can be found for a given mixture concentration $\vec{c}$ and the phase concentrations can be expanded around these concentration (see [2,17]):

$$\Delta\vec{c}_\alpha = \vec{c}_\alpha - \vec{c}^{\,0}_{\alpha\beta}. \tag{27}$$

Again, using the equality of chemical potentials (26), we have

$$\Delta\vec{c}_\alpha = \Delta\vec{c}_\beta\frac{\partial\vec{c}_\alpha}{\partial\vec{c}_\beta} = \Delta\vec{c}_\beta\frac{\partial f_c^\beta}{\partial f_c^\alpha}\frac{\partial\vec{c}_\alpha}{\partial\vec{c}_\beta} = \Delta\vec{c}_\beta\frac{f_{cc}^\beta}{f_{cc}^\alpha} =: \Delta\vec{c}_\beta\vec{\vec{k}}_{\alpha\beta}. \tag{28}$$

The abbreviation $f_c^\alpha = \frac{\partial f_\alpha}{\partial\vec{c}_\alpha}$ is used and the generalized partition coefficient $\vec{\vec{k}}_{\alpha\beta}$ is introduced. Using (3), (27) and (28), we can now eliminate the phase concentrations from (25):

$$\dot{\vec{c}} = \nabla\left(\sum_{\alpha=1}^{N}\phi_\alpha\vec{\vec{D}}_\alpha\nabla\frac{\left(\vec{c} - \sum_{\beta=1}^{N}\phi_\beta\left(\vec{c}^{\,0}_{\beta\alpha}\vec{\vec{k}}_{\beta\alpha}\vec{c}^{\,0}_{\alpha\beta}\right)\right)}{\sum_{\beta=1}^{N}\phi_\beta\vec{\vec{k}}_{\beta\alpha}}\right). \tag{29}$$

This equation has the same form as Eq. (40) in [11], but with a different model for the diffusion matrix. The more important fact is that the unknowns $\vec{c}_\alpha$ are eliminated using the local linearization (27). Hence, it is very effective to solve it numerically. It is not restricted to the dilute solution limit, applicable to an arbitrary number of components and phases. Updating the constants if the applicability of the linear expansion (27) is violated, the model is applicable to arbitrary phase diagrams. With slight modifications, stoichiometric phases can also be treated [2].

The displacements are defined from the principle of relaxation into mechanical equilibrium Eq. (18). Numerically, this equation is solved for the displacement vector u^i, $\epsilon^{ij} = \frac{1}{2}(\frac{\partial}{\partial u^i}u^i + \frac{\partial}{\partial u^j}u^j)$, in the weak formulation using linear finite elements. The displacements are located at the corners of a square control volume grid and the physical properties are approximated to be constant over the control volume. The boundary conditions are free volume expansions (or contractions), but keeping the rectangular shape of the calculation box. This is done in a three-step procedure: We define the total strain ϵ^{ij} as the sum of a relative or test strain $\tilde{\epsilon}^{ij}$ and an average strain $\bar{\epsilon}^{ij}$: $\epsilon^{ij} = \tilde{\epsilon}^{ij} + \bar{\epsilon}^{ij}$. First, relative displacement $\tilde{u}^i$ and relative strain $\tilde{\epsilon}^{ij}$ is calculated with fixed

[1] It shall be noted that, for numerical convenience, Eq. (19) is usually treated in the antisymmetric approximation of [1].

[2] Note that the $\vec{c}^{\,0}_{\alpha\beta} = \vec{c}^{\,0}_{\alpha\beta}(x^i, t)$ are, like the other functional variables, functions in space and time.

boundaries. Second, the average strain $\bar{\epsilon}^{ij}$ is calculated from the principle that the variation of the elastic energy with respect to the average strain has to vanish in mechanical equilibrium:

$$\bar{\epsilon}^{ij} = \int \bar{C}^{mnkl}(\tilde{\epsilon}^{mn} - \epsilon^{*mn}) \left[\int \bar{C}^{klij} \right]^{-1}. \tag{30}$$

In the last step, the box is expanded (or contracted) with the average strain. The procedure assumes that the relative strain $\tilde{\epsilon}$ is independent of the average strain $\bar{\epsilon}$, which is not true in general. Therefore it has to be iterated. As in the cases treated here, the time discretization, due to the coupling with the phase field equation, is high and the increments of $\bar{\epsilon}$ are small, only one iteration step, as described, was used. It is also straightforward to consider external forces using this procedure.

The phase field and concentration equations are solved using a standard control volume technique on a square grid and explicit time stepping; the strain equation is solved implicitly using finite elements on the same grid. The coupling between the equations is treated explicitly.

5. Test against an analytical solution

To test the numerical implementation and the dependence of the results on the numerical resolution of the simulation, we investigate the case of a single spherical particle in an infinite matrix. The analytical solution (in direction x^1 from the center of the particle) is given by Eshelby [18] for isotropic elasticity data, equal in both phases:

$$\sigma^{ii} = \begin{cases} -\sigma_0 \text{ inside the particle; } x^1 < r_p \\ -\sigma_0 \left(\dfrac{r_p}{x^1}\right)^3 \quad \text{for } i = 1;\ x^1 > r_p \\ \dfrac{1}{2}\sigma_0 \left(\dfrac{r_p}{x^1}\right)^3 \quad \text{for } i \neq 1;\ x^1 > r_p \end{cases} \tag{31}$$

$$\sigma_0 = \frac{2}{3}(C_{11} + 2C_{12})\frac{1-2\nu}{1-\nu}\epsilon^*. \tag{32}$$

We use data in the range of those for low alloyed steel: $C_{11} = 280$ GPa, $C_{12} = 120$ GPa, corresponding to an elasticity modulus $E = 208$ GPa and a Poisson ratio $\nu = 0.3$. The eigenstrain ϵ^* is 1% and the particle radius is taken as $r_p = 1.4$ μm. σ_0 is 1980 MPa for the given data. The calculations were performed in a cubic domain of $15 \times 15 \times 15$ μm^3 with discretizations Δx ranging from 0.05 μm to 0.3 μm (the calculation with the highest discretization was conducted only in one quadrant of the domain and using symmetric boundary conditions). The interface width η was $6\Delta x$ in all calculations and thereby varies with the discretization. Fig. 2 gives the normal σ^{11} and tangential σ^{33} stresses in a radial direction from the origin of the particle; the shear component σ^{13} is identical to 0 in this direction. The following observations are to be made:

- Both normal and tangential stresses reach the correct level in the center of the particle within less than one percent accuracy for all discretizations.
- Both normal and tangential stresses follow the correct stress distribution outside the particle AND outside the interface region within a few percent accuracy.

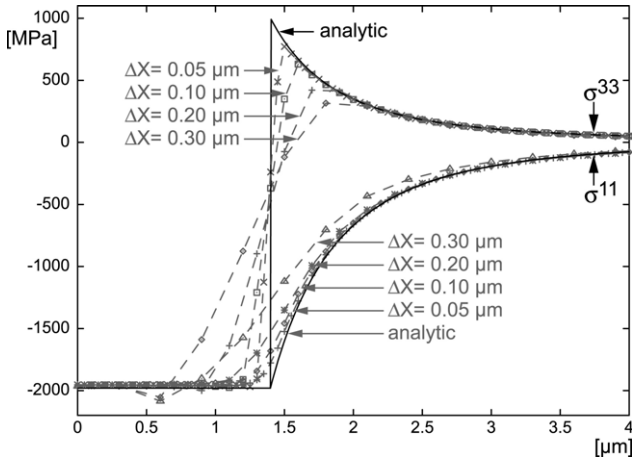

Fig. 2. Calculated normal (σ_{11}) and tangential (σ_{33}) stresses in a radial direction from the center of the particle for different discretizations in comparison with the analytical solution Eq. (31).

- Inside the diffuse interface, the stress distributions are smoothed out, as is usual for diffuse interface models. For the low discretization, where the interface width reaches the particle radius, the normal stress undershoots the analytical value inside the particle before converging to the correct value.
- Because of the smoothing out, the tangential stress does not reach the correct maximum at the sharp interface position value for all discretizations. It increases from 30% for the lowest discretization to 70% for the highest discretization.
- Both stress components converge to the analytical limit (continuous for σ^{11} and discontinuous for σ^{33}) with decreasing interface width. The influence of curvature pressure is not included in the model.

From these observations, we can conclude that the results of the presented model with the chosen numerical implementation converge to the analytical solution if the discretization is sufficiently high. If the peak value of the tangential stress at the interface is of key interest, e.g. for the investigation of fracture, it might become difficult to reach sufficient accuracy. For the investigation of the effect of transformation strain on phase transformations, however, the elastic contribution to the phase evolution ΔG^{EL}, Eq. (23), is of key interest. Evaluation of (23) in average over the interface gives similar values for all calculations of $30\frac{\mathrm{J}}{\mathrm{cm}^3}$ with a slightly increasing tendency with discretization. The total variation of ΔG^{EL} between the calculations is 9%, which is astonishing because of the large deviation of the peak stresses from the sharp interface solution. Obviously, the volumetric description of the interface energies supports the independence of ΔG^{EL} of the discretization and thereby of the interface width.

6. Growth of a single ferrite particle in an austenite matrix

In this section, we will discuss the effect of elastic strain energy on the ferrite (α) to austenite (γ) transformation in a ternary Fe–C0.463at%–Mn0.496at% alloy. The mechanical data are identical to the calculations in the previous section.

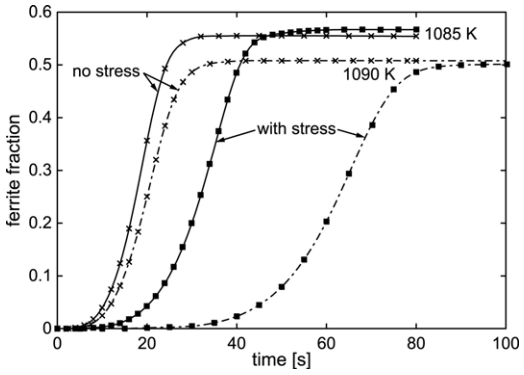

Fig. 3. Ferrite fraction as a function of time for an isothermal transformation at 1090 K and 1085 K, with and without elastic interaction.

The chemical Gibbs energies are taken from the TCFE3 database [19]. The diffusion coefficients of carbon and manganese are $D^{\gamma}_{\mathrm{C}} = 2 \times 10^{-8}$ cm^2 s^{-1} and $D^{\gamma}_{\mathrm{Mn}} = 4.1 \times 10^{-14}$ cm^2 s^{-1}, respectively. The interfacial energy and mobility were taken as isotropic, $\sigma = 5 \times 10^{-5}$ J/cm^2 and $\mu = 1 \times 10^{-5}$ cm^4/J s. The domain size was $62 \times 62 \times 62$, cells with a discretization of $\Delta x = 0.25\ \mu m$. The interface width is $\eta = 6$ cells. This domain size is of the order of the austenitic grain size in a fine-grained austenitic steel. For the displacements, free expansion parallel to the Cartesian axes with a fixed origin are allowed as boundary conditions. The phase field and concentration obey periodic boundary conditions. The phase field equation (19), concentration equation (25) and strain equation (18) are solved step by step with a time discretization between 10^{-2} s and 10^{-3} s, depending on the discretization. Instantaneous relaxation to mechanical equilibrium is assumed for every time step, according to Eq. (18).

At first, we will discuss an isothermal transformation at 1090 K and 1085 K, 25 K and 40 K below the $\gamma \rightarrow \alpha$ equilibrium temperature of the material. An initial ferrite grain with a radius close to zero is set in the center of an austenitic matrix. Because the phase field equation requires a minimal structure size of twice the interfacial thickness η to reproduce the growth kinetic of the sharp interface problem, Eq. (19) is solved without the curvature related part until the particle radius reaches η. Using this procedure, the initial growth is governed by thermodynamic and elastic forces only. Curvature undercooling is considered when the seed exceeds a size of 2η.

Fig. 3 shows the transformation curves (ferrite fraction as a function of time) for the two cases with and without elastic energy interaction, respectively. Next, Fig. 4 sketches the ferrite grain for three corresponding times during transformation.

The ferrite seed grows at the cost of the austenite, while carbon segregates into the austenitic matrix. The kinetics of the transformation in the case without elastic interaction is controlled by carbon diffusion and the finite mobility of the interface (for more details about the process, see [20,21]). Switching on the elastic interaction leads to a decrease of the kinetics, as the expanding ferritic grain has to work against the austenite matrix. However, as the transformation continues, the austenitic matrix shrinks in thickness and loses its elastic strength, i.e. the compressive forces on the ferrite decrease. If the fraction of ferrite exceeds approximately 50%, the transformation is even enhanced compared to the case without elastic interaction, as the elastic energy of the system now decreases with increasing transformation. To illustrate this further, Fig. 5 gives the chemical and elastic contributions to the total driving force over time, averaged over the interface, as well as the effective driving force which is the sum over these contributions. A negative sign means a driving force in favor of the transformation $\gamma \rightarrow \alpha$. At the beginning of the transformation, only the chemical contribution is in favor of the transformation, while curvature (not determined) and

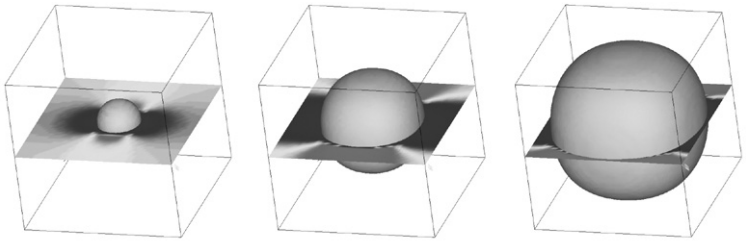

Fig. 4. Growing ferrite grain (phase field 0.5 isoplane) after 40 s, 60 s, and 80 s of transformation. σ_{yy} normal stress is visualized on the cutting plane.

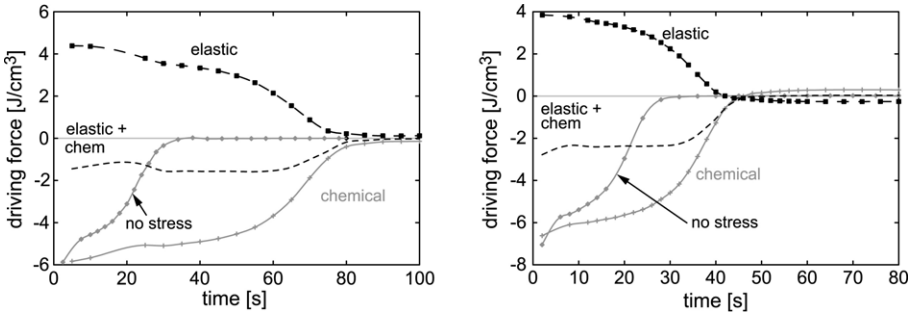

Fig. 5. Local driving force contributions at the interface as a function of time. Left: transformation at 1090 K. Right: transformation at 1085 K.

elastic strain work against it. The elastic (back) driving force decreases with time. This reflects the fact that the surrounding austenite shell becomes thinner. At 1090 K, the transformation stops at 50% ferrite compared to 50.8% in the case of disabled elastic interaction. This difference is due to the residual elastic driving force. For a transformation at lower temperature, the ferrite becomes the majority phase and the elastic driving force becomes negative after 40 s. Consequently, the transformation is driven beyond chemical stability, i.e. the chemical driving force becomes positive. Obviously, the total driving force as the sum over both contributions vanishes in the equilibrium state.

The deviation of the total equilibrium state from chemical equilibrium state is thereby an effect of the γ/α composite structure, where the elastic energy stored in the system is a maximum at around 50% ferrite fraction. Because the ferrite-to-austenite ratio is determined by the equilibrium conditions for each temperature, this finite size effect does not depend on the domain size but is an inherent property of a two-phase structure. The exact value of the maximum will depend on the morphology of the phase distribution on the one hand and differences in elastic constants between the phases on the other hand. The majority phase is favored by the elastic energy as, in the finite system, the total balance of stresses leads to an accumulation of stress in the minority phase (finite in this context means the size of one cell in a semi-periodic multi grain structure, idealized by our one-particle system). The effect is summarized in Fig. 6. The figure compares the equilibrium fractions of ferrite for various temperatures considering chemical contributions only and considering chemical and elastic contributions. The elastic interaction suppresses the transformation for alloys with chemical equilibrium fraction below ∼50% and enhances the transformation for alloys with chemical equilibrium fraction above ∼50%. This is the most important practical finding of the work. One may note that this effect also depends on the boundary conditions and only becomes effective when the volume can expand freely. In addition, one must consider that the thermophysical data, as stored in the thermodynamic database, are deduced from measurements that already contain the effect of transformation strain and elastic energy. Thus, in the calculations, the elastic energy will be overestimated. It will be a task for the future to separate chemical and elastic contributions in thermodynamic databases. As a last aspect, in reality, at temperatures around 1000 K, plasticity has to be taken into account to get quantitative results.

As a kind of outlook, Figs. 7 and 8 show the calculated phase and hydrostatic stress distributions in a multi grain structure in 2D, transformation at 1075 K. The matrix consists of 16 austenite grains. 22 ferrite grains are nucleated at the triple junctions. Cubic anisotropy is considered in the elastic constants. On the left, the intermediate structure for a ferrite fraction of 25% is shown. The right-hand pictures show the structure at the end of transformation with a ferrite fraction of 63%. A first observation from these calculations is that the effect of transformation strain hampers the coalescence of ferrite grains that are surrounded by a band of high tensile strain. Thus in the grain structure, calculated with elastic

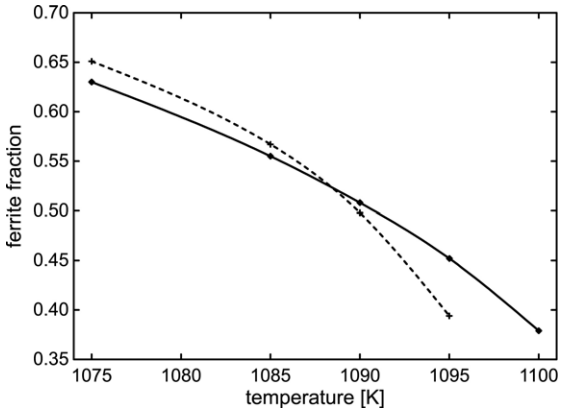

Fig. 6. Final ferrite fraction as a function of transformation temperature.

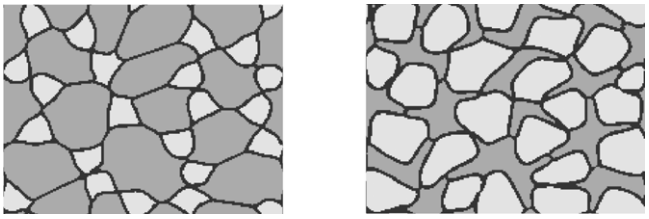

Fig. 7. Phase distribution in a polycrystalline austenite/ferrite structure. Light grey indicates ferrite; medium grey austenite: 200 × 150 cells, 40 × 30μm^2. Left-hand side: ferrite fraction 25%. Right-hand side: ferrite fraction 63%.

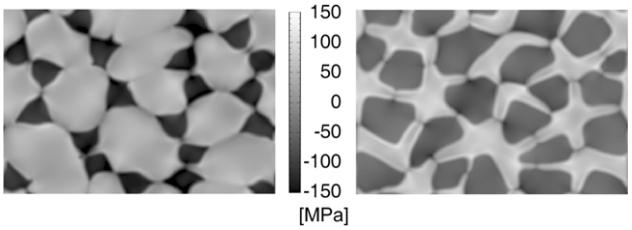

Fig. 8. Hydrostatic stress distribution within the structures of Fig. 7. Stress levels are in between −150 MPa and 150 MPa.

interaction, the matrix character of the austenite is more pronounced than in the case when transformation strain is neglected.

7. Conclusion

A multi phase field method is presented that includes elastic interactions between the phases. The model takes the elastic constants as a function of the phases. It can be applied to materials with arbitrary elastic properties and eigenstrains. A new interface condition is derived that conserves mechanical equilibrium between the phases in the diffuse interface region and triple junctions. Hence, it is consistent with the philosophy of the multi phase field method. The numerical implementation of the model is tested against an analytical solution. It is shown that insufficient resolution of the interface will lead to a truncation of the maximum stress in the interface. The elastic driving force for the phase transformation, however, is quite insensitive to discretization. The demand for high discretization is therefore relaxed with respect to the transformation behavior.

Application of the model to γ/α transformation in an iron–carbon–manganese alloy demonstrates the importance of elastic energy on the transformation kinetics and the equilibrium fraction of a dual-phase alloy. This, however, has to be interpreted carefully, as plastic deformations, which certainly play a role at the temperatures of transformation, are not taken into account and the thermophysical data used do not separate chemical and elastic contributions in the Gibbs free energy description.

Acknowledgments

This work was funded by the European Commission under framework 5 project 'VESPISM' and by the German research foundation DFG under the integrated projects SPP 1168 and SFB 370.

References

[1] I. Steinbach, F. Pezzolla, B. Nestler, M. Seeßelberg, R. Prieler, G.J. Schmitz, J.L.L. Rezende, A phase field concept for multiphase systems, Physica D 94 (1996) 135–147.
[2] J. Tiaden, B. Nestler, H.J. Diepers, I. Steinbach, The multiphase-field model with an integrated concept for modeling solute diffusion, Physica D 115 (1998) 73–86.
[3] I. Steinbach, F. Pezzolla, A generalized field method for multiphase transformations using interface fields, Physica D 134 (1999) 385.
[4] L.-Q. Chen, Phase-field models for microstructure evolution, Annu. Rev. Mater. Res. 32 (2002) 113–114.
[5] K. Kassner, Ch. Misbah, J. Müller, J. Kappey, P. Kohlert, Phase-field modeling of stress-induced instabilities, Phys. Rev. E 63 (2001) 036117-27.
[6] W. Dreyer, W.H. Müller, A study of the coarsening in tin/lead solders, Int. J. Solids Struct. 37 (2000) 3841.
[7] G. Caginalp, P. Fife, Phase-field methods for interfacial boundaries, Phys. Rev. B 33 (1986) 7792–7794.
[8] G. Caginalp, X. Chen, Phase field equations in the singular limit of sharp interface problems, IMA Vol. Math. Appl. 43 (1990) 1–28.
[9] A. Karma, W.-J. Rappel, Phase-field method for computational efficient modeling of solidification with arbitrary interface kinetics, Phys. Rev. E 53 (1996) 3017–3020.
[10] A. Karma, Phase-field formulation for quantitative modeling of alloy solidification, Phys. Rev. Lett. 87 (11) (2001) 115701.
[11] S.G. Kim, W.T. Kim, T. Suzuki, Phase-field model for binary alloys, Phys. Rev. E 60 (6) (1999) 7186–7197.
[12] A. Reuss, Berechnung der Fießgrenze von Mischkristallen auf Grund der Plastizitätsbedingung für Einkristalle, Z. Angew. Math. Mech. 9 (1) (1929) 49–58.
[13] R. Hill, Elastic properties of reinforced solids: Some theoretical principles, J. Mech. Phys. Solids 11 (1963) 357–372.
[14] W. Voigt, Über die Beziehung zwischen den beiden Elastizitätskonstanten isotroper Körper, Ann. Phys. Chem. 38 (1889) 573–587.
[15] Y.U. Wang, Y.M. Jin, A.G. Khachaturyan, Phase field microelasticity theory and modeling of elastically and structurally inhomogeneous solid, J. Appl. Phys. 92 (3) (2002) 1351–1360.
[16] J. Eiken, B. Böttger, I. Steinbach, Multiphase-field approach for multicomponent alloys with extrapolation scheme for numerical application, Phys. Rev. E (2006) (in press).
[17] J. Tiaden, U. Grafe, I. Steinbach, The prospectives of phase field modelling for the investigation of phase transformations in steel, in: Cutting Edge of Computer Simulation of Solidification and Casting, ISBN: 4-930980-01-1C3057, 1999, pp. 13–20.
[18] J.D. Eshelby, The determination of the elastic field of an ellipsoidal inclusion, and related problems, Proc. Roy. Soc. A 241 (1957) 376–396.
[19] http://www.thermocalc.se.
[20] G. Pariser, P. Schaffnit, I. Steinbach, W. Bleck, Simulation of the $\gamma \rightarrow \alpha$ transformation using the phase–field method, Steel Res. 72 (9) (2001) 354–360.
[21] M.G. Mecozzi, J. Sietsma, S. van der Zwaag, M. Apel, P. Schaffnit, I. Steinbach, Analysis of the $\gamma \rightarrow \alpha$ transformation in a C–Mn steel by phase field modelling, Metall. Trans. A 36 (2005) 2327–2340.